Soil organic carbon and particle sizes mapping using vis–NIR, EC and temperature mobile sensor platform

ARTICLE *in* COMPUTERS AND ELECTRONICS IN AGRICULTURE · JUNE 2015

Impact Factor: 1.76 · DOI: 10.1016/j.compag.2015.03.013

4 AUTHORS:

Maria Knadel

Aarhus University

20 PUBLICATIONS **62** CITATIONS

SEE PROFILE

A. Thomsen

Aarhus University

53 PUBLICATIONS **848** CITATIONS

SEE PROFILE

Kirsten Schelde

Aarhus University

54 PUBLICATIONS **1,062** CITATIONS

SEE PROFILE

Mogens H. Greve

Aarhus University

78 PUBLICATIONS **381** CITATIONS

SEE PROFILE

Computers and Electronics in Agriculture 114 (2015) 134–144

Contents lists available at ScienceDirect

Computers and Electronics in Agriculture

journal homepage: www.elsevier.com/locate/compag

Soil organic carbon and particle sizes mapping using vis–NIR, EC and temperature mobile sensor platform

Maria Knadel *, Anton Thomsen, Kirsten Schelde, Mogens Humlekrog Greve

Dept. of Agroecology, Faculty of Science and Technology, Aarhus University, Blichers Allé 20, PO Box 50, DK-8830 Tjele, Denmark

ARTICLE INFO

Article history:
Received 4 September 2014
Received in revised form 16 March 2015
Accepted 17 March 2015

Keywords:
Mobile sensors
NIRS
EC
PLS
SOC
Soil particle sizes

ABSTRACT

Soil organic carbon (SOC) is an important parameter in the climate change mitigation strategies and it is crucial for the function of ecosystems and agriculture. Particle size fractions affect strongly the physical and chemical properties of soil and thus also SOC. Conventional analyses of SOC and particle sizes are costly limiting the detailed characterization of soil spatial variability and fine resolution mapping. Mobile sensors provide an alternative approach to soil analysis. They offer densely spaced georeferenced data in a cost-effective manner. In this study, two agricultural fields (Voulund1 and Voulund2) in Denmark were mapped with the Veris mobile sensor platform (MSP). MSP collected simultaneously visible near infrared spectra (vis–NIR; 350–2200 nm), electrical conductivity (EC: shallow; 0–30 cm, deep; 0–90 cm), and temperature measurements. Fuzzy k-means clustering was applied to the obtained spectra to partition the fields and to select representative samples for calibration purposes. Calibration samples were analyzed for SOC and particle sizes (clay, silt and sand) using conventional wet chemistry analysis. The objectives of this study were to determine whether it is the single sensors or the fusion of sensor data that provides the best predictive ability of the soil properties in question. Using partial least square regression (PLS) excellent calibration results were generated for all soil properties with a ratio of performance to deviation (RPD) values above 2. The best predictive ability for SOC was obtained using a fusion of sensor data. The calibration models based on vis–NIR spectra and temperature resulted in RMSECV = 0.14% and R^2 = 0.94 in Voulund1. In Voulund2, the combination of EC, temperature and spectral data generated a SOC model with RMSECV = 0.17% and R^2 = 0.93. The highest predictive ability for clay was obtained using spectral data only in Voulund1 (RMSECV = 0.34% and R^2 = 0.76). Whereas in Voulund2, improved results were obtained after combining spectral and temperature data RMSECV = 0.20% and R^2 = 0.92. The best predictions of silt and sand were obtained when using spectral data only and resulted in RMSECV = 0.35%, R^2 = 0.82 and RMSECV = 0.85%, R^2 = 0.81, respectively, in Voulund1 and RMSECV = 0.31%, R^2 = 0.86 and RMSECV = 0.74%, R^2 = 0.92, respectively, in Voulund2.

The best models were used to predict soil properties from the field spectra collected by the MSP. Maps of predicted soil properties were generated using ordinary kriging. Results from this study indicate that robust calibration models can be developed on the basis of the MSP and that high resolution field maps of soil properties can be compiled in a cost-effective manner.

1. Introduction

1.1. Soil organic carbon and particle sizes

Soil organic carbon (SOC) is an important parameter in the climate change mitigation strategies as it plays a key role in the global carbon cycle. Moreover, it is crucial for the function of ecosystems and agriculture. It affects soil biological, physical and chemical functions, having therefore a major influence on soil structure, ability to store water and form complexes with metal ions and to supply nutrients. Soil particular size distribution is

Abbreviations: A, absorbance (log 1/*R*, where *R* is reflectance); EC, electrical conductivity; EC-sh, shallow electrical conductivity; EC-dp, deep electrical Conductivity; MIR, mid-infrared; MSP, multi-sensor platform; MSEP, mean standard error of prediction (in kriging validation); MSC, multiplicative scatter correction; NIR, near infrared; NIRS, near infrared spectroscopy; OM, organic matter; PCA, principal component analysis; PLS, partial least squares regression; RMSECV, root mean square error of cross-validation; RPD, the ratio of standard error of prediction to standard deviation; SD, standard deviation; SOC, soil organic carbon; SNV, standard normal variate; VIS, visible.

* Corresponding author. Tel.: +45 8715 7615.
E-mail address: maria.knadel@agrsci.dk (M. Knadel).

http://dx.doi.org/10.1016/j.compag.2015.03.013
0168-1699/

another important property of soil having both environmental and agricultural implications. It has effects on water holding capacity, nutrient retention and supply, drainage and nutrient leaching. Consequently, reliable techniques for measuring and mapping SOC and particle sizes are necessary in precision agriculture for decision-support systems and in sustainable land management practices. However, the conventional wet chemistry analyses of soil are costly what limits detailed characterization of spatial variability of soil and the possibility to create precise and fine resolution soil maps. Thus, alternative approaches are required.

1.2. Visible near infrared spectroscopy and electrical conductivity

Visible Near infrared (vis–NIR) spectroscopy is a rapid and cost-effective method which has been used for soil analysis since mid-1990s. Vis–NIR spectra carry information on organic and inorganic soil materials, particle size, color and water content. The technique employs measurements of photon energy in the wavelength range 350-2500 nm. Especially mobile vis–NIRS sensors for soil characterization are attracting increasing attention due to their potential for applications to e.g. precision agriculture or soil mapping in general. The first application of on-the-go spectroscopic sensors was reported by Shonk et al. (1991) followed by a study including a prototype portable vis–NIRS sensor developed by Hummel et al. (1996). Since then, prediction of a range of soil constituents has been tested using a variety of mobile sensors. The predictive abilities of mobile sensors vary significantly and depend on the type of data fused, soil spatial variability, the concentrations, and the ranges of the soil attributes (Stenberg and Viscarra Rossel, 2010). Unlike the well-controlled conditions imposed for laboratory measurements, many less controllable factors can affect the quality of in-situ acquired data such as soil particle size and aggregation, soil roughness, soil temperature, sensor-to-soil distance, vibrations, dust, plant residues, pebbles and stones but also confounding factors such as variation in soil mineralogy, moisture, organic matter and their interactions (Morgan et al., 2009; Shonk et al., 1991).

Soil electrical conductivity (EC) is another sensing technique and one of the most frequently used measurements for characterizing soil variability at field scale for precision agriculture because of its reliability, accuracy, high number of measurements and ease of collecting the data (Corwin and Lesch, 2003). It can be measured using electromagnetic induction or galvanic contact resistivity methods. EC is a function of the soil physical and chemical properties, soil salinity, saturation, water content and bulk density (Corwin and Lesch, 2003). It has been therefore widely used for mapping the variation in soil particle sizes, salinity, water content, bulk density, organic matter (OM) and temperature (Broge et al., 2004; Corwin and Lesch, 2005; Domsch and Giebel, 2004; Kochanowski et al., 1988; Lück et al., 2009; Lund et al., 1999; Moral et al., 2010; Sudduth et al., 2005). Moreover, it was found that EC increases 1.9% per 1 °C (Corwin and Lesch, 2005). Thus, soil temperature can be correlated to EC and easily used as additional variable in soil mapping.

1.3. Sensor data fusion

Mobile sensors such as vis–NIRS or EC sensors, can generate the densely spaced geo-referenced data in a cost-effective manner necessary for capturing soil spatial variability and are therefore, powerful tools for landscape-scale soil characterization (Malley et al., 2004). However, when using only one sensor it is not possible to measure all soil properties. Viscarra Rossel et al. (2011) listed a number of benefits from using a multi-sensor compared to a single-sensor system. The most important benefits were: robust operational performance, increased confidence of the acquired data due to different sensors measuring the same soil, extended attributes coverage, and increased dimensionality of the measurement space. Thus, for improved estimation of soil properties a fusion of conceptually different mobile sensors has been investigated in some studies. Knadel et al. (2011) reported on mobile soil sensor data fusion using the Veris mobile sensor platform (MSP) consisting of an optical shank-based vis–NIR (visible-near infrared) sensor and EC measurements to map soil organic carbon (SOC) within a partly highly variable field in Denmark. Improved SOC calibrations were obtained by fusing EC with spectral data. They generated a detailed map of SOC based on a significantly lower number of calibration soil samples than needed for conventional mapping based on grid sampling. In another study, Schirrmann et al. (2011) used the Veris mobile platform with additional pH meter for mapping macronutrients at two fields in Northern Germany. However, poor predictive abilities of the generated partial least square (PLS) regression models were reported. Further they concluded that the fusion of sensor data improved only the pH mapping results.

1.4. Soil analysis and mapping in Denmark

The existing information on soil properties in Denmark was obtained in the mid 70s during the Danish Soil Classification (Madsen et al., 1992). Not only is this information outdated but the data has also insufficient spatial resolution (1:50,000) for management on a field scale. Hence, new soil data must be collected and reflect the current soil properties on specific field, and at a specific location in this field. Detailed information of such soil properties as SOC and particle sizes can help Danish farmers to gain a better insight on the quality of their soil and support decision making to achieve higher yields. Moreover it can be used in the environmental regulation of agricultural production and will to a great extent help Denmark to fulfill the responsibilities of the Kyoto protocol from 1997.

To supplement the time-consuming and costly conventional approach to soil survey in Denmark, a method for SOC and particle sizes mapping employing the use of vis–NIR, EC and temperature sensors was investigated. Considering the advantages of NIRS and EC sensing techniques in combination with a mobile sensor platform for soil surveying the objective of this study was to test the feasibility of using the Veris MSP for simultaneous mapping of SOC, clay, silt and sand contents of two agricultural fields in Western Denmark. In search of robust calibrations we tested EC, temperature, and vis–NIR spectral data individually, and different combinations of these predictors for each soil property and field separately. As a final result prediction maps of soil properties were generated using ordinary kriging interpolation.

2. Materials and methods

2.1. Study site

The study sites are located in Western Denmark within Voulund farm (800 ha) (Fig. 1) which is producing mainly pigs, feed crops and maize. The two investigated sites (Voulund1–13.7 ha and Voulund2–12.7 ha) represent homogenous agricultural fields adjacent to each other with Voulund1 located north of Voulund2. The fields were planted with winter barley. The climate in this region is temperate-maritime with an average precipitation of 781 mm/year and mean annual temperature of 7.5 °C (Danish Meteorological Institute, verified August 2011). The soil type is a Spodosol located on the glaciofluvial sandy outwash plains of the most recent European glaciations (Schelde et al., 2011).

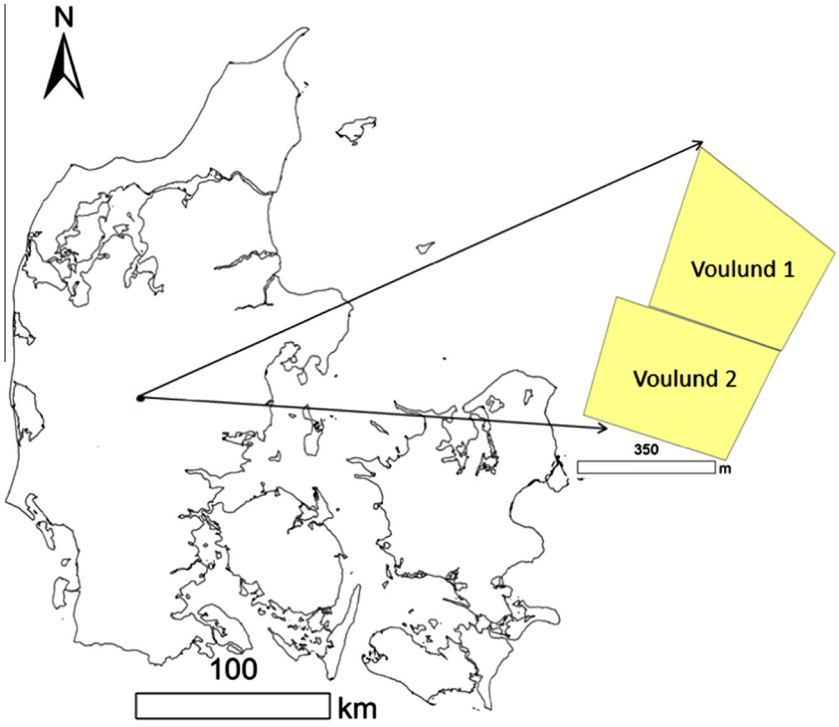

Fig. 1. The location of the two study fields: Voulund1 and Voulund2 (1, 5 column fitting image).

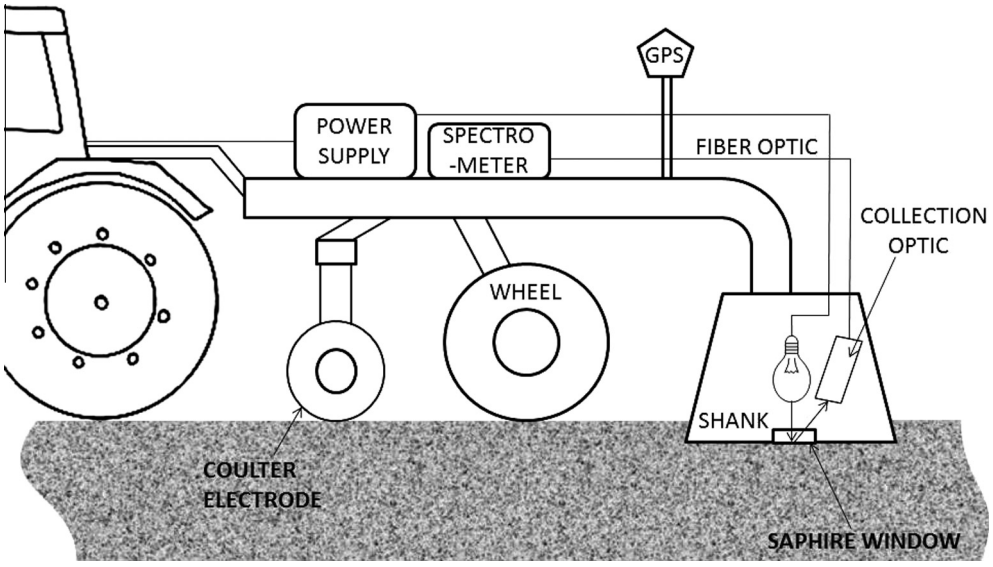

Fig. 2. Schematic drawing of the Veris multi-sensor platform (2 column fitting image).

2.2. Multi-sensor platform (MSP) data collection

Measurements were collected using a mobile MSP developed by Veris Technologies, Kansas, USA. A field survey was conducted on the 10th of October (Voulund1) and on the 11th of October 2012 (Voulund2). Sensors were mounted on the Veris toolbar and pulled by a tractor (Fig. 2) driving approximately 5 km/h along 12 m spaced transects. Vis–NIR measurements were collected from a shank pulled in the soil at a depth of approximately 5 cm. The sensors used were an Ocean Optics (USB4000-VIS–NIR, Ocean Optic Instruments Inc., Dunedin, FL, USA) charge-coupled device (CCD) array at 350–1050 nm and a Hamamatsu (C9914GB TG-Cooled NIR II, Hamamatsu, Shizuoka, Japan) InGaAs linear image sensor at 900–2200 nm. Detailed information about the sensors can be found in Knadel et al. 2013. Soil temperature measurements were collected with an infrared sensor placed in an open cavity at the bottom of the shank. Electrical conductivity data was obtained simultaneously from six coulter electrodes (dual-depth arrays) placed at the front of the toolbar recording electrical conductivity at two depths: shallow (EC-sh) at approximately 0–30 cm and deep (EC-dp) at approximately 0–90 cm (Fig. 2). Injection electrodes were 69 cm from each other, 21.8 cm from the inner receiver electrodes (for EC-sh measurements), and 28.7 cm from outer electrodes (for EC-dp measurements).

Approximately 20 measurements per second were taken and averaged into one. Each data point was geo-referenced with a real-time kinematic GPS of a few centimeters accuracy.

2.3. Soil sampling and laboratory analysis

A total of 30 sampling locations (15 from each field) were selected for calibration purposes. The selection procedure for calibration samples was done following the protocol described by Christy (2008). In short, to determine representative sampling locations from the acquired spectral data, soil spectra were first compressed with a principal component analysis (PCA). Samples with a Mahalanobis distance $\geqslant 3H$ (H is the leverage statistic) were considered as outliers and removed. A fuzzy c-means algorithm was applied to cluster spectral data into 15 spatial clusters separately for each field. Within each cluster a location was chosen so that it was close to the center of the cluster in spectral data space and was geographically surrounded by most points from the same cluster (Fig. 3). Knadel et al. (2013) investigated the effects of sample number on the predictive ability of PLS calibration models for a highly heterogeneous field in Denmark. The authors showed that 15 representative calibration samples for a 14.6 ha field provided acceptable results for SOC and texture predictions, reducing significantly the costs of reference sampling and analysis.

The two Voulund fields can be characterized as relatively homogenous in terms of soil properties and are of a similar size as the one of Knadel et al. (2013). Therefore, an equally low number of calibration samples should sufficiently cover their variability. Considering the low number of calibration samples it is of important to cover the variability of the collected spectra and thus, the fields. Following Christy (2008) and Knadel et al. (2011) soil samples were collected from the furrow left by the shank and used for reference analysis. SOC was analyzed using a LECO analyzer coupled with an infrared CO_2 detector (Thermo Fisher Scientific Inc., USA) and soil texture (clay, silt, sand) was determined by a combined sieve/hydrometer method (Dane and Topp, 2002). Clay was defined as particles <2 μm, silt 2–63 μm, fine sand 63–200 μm, and coarse sand 200–2000 μm.

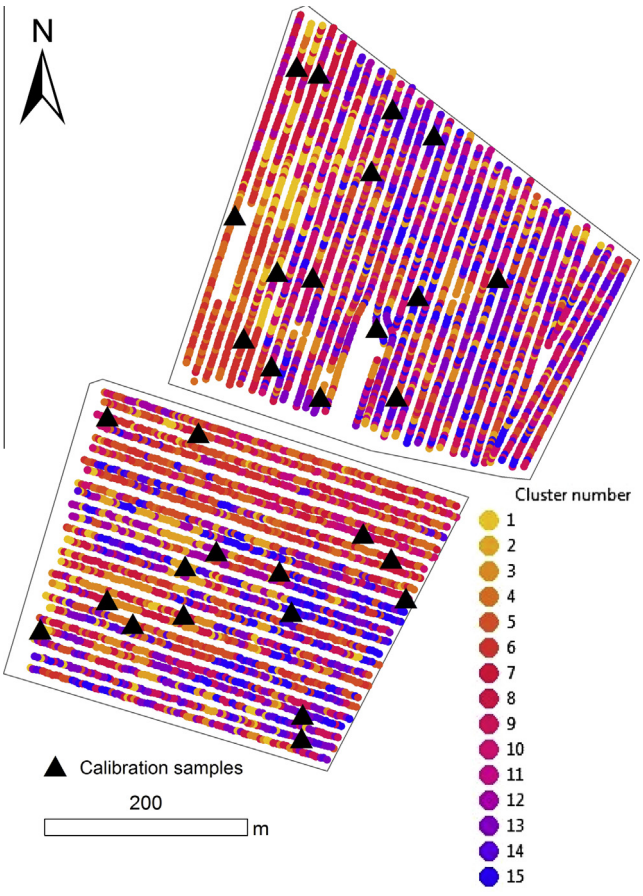

Fig. 3. Measurement transects and soil sampling locations. Data points colored according to cluster number (1, 5 column fitting image).

2.4. Spectral preprocessing

In order to improve the results of regression modeling, several standard pre-processing methods can be applied to spectral data to account for nonlinearities, measurement and sample variation, and noise. It is not possible to specify a universal pre-processing method suitable for all applications. The type of pre-processing needed is data-dependent and needs to be decided upon using a trial and error approach. Both chemical and structural differences in the sample can lead to non-linear scatter effects. For linearization of the relationship between absorbance and concentration, measured reflectance (R) was transformed to log $1/R$ (Stenberg and Viscarra Rossel, 2010). The standard pre-processing techniques included scatter corrections and derivations (Rinnan and Rinnan, 2007). Multiplicative scatter correction (MSC) was used to remove additive and multiplicative effects present in the data. Like MSC, the standard normal variate (SNV) transform was applied to remove multiplicative interferences of scatter and particle size effects from spectral data. Additional detrending calculated a baseline function as a least squares fit of a polynomial to the sample spectrum. Derivatives were applied to correct for baseline effects in spectra for the purpose of removing nonchemical effects and creating robust calibration models. The first derivative of a spectrum is a measure of the slope of the spectral curve. The slope of the curve is not affected by baseline offsets in the spectrum. Thus the first derivative is a very effective method for removing baseline offsets. The second derivative is a measure of the change in the slope of the curve. In addition to ignoring the offset, it is unaffected by any linear "trend" that may exist in the data, and is therefore an effective method for removing the baseline offset and slope from a spectrum. The 1st and the 2nd Savizky-Golay derivatives were applied to the data sets with a second polynomial order with 11 smoothing points.

2.5. Calibration model development

Partial least square regression (PLSR) was applied to generate calibration models between the predictors (sensor data) and the soil properties, separately for each field. It is one of the most commonly used regression methods and produces satisfactory calibration results for a variety of soil constituents. It models the predictors (e.g. sensor data) and the response variable (e.g. soil property of interest) simultaneously to find the latent variables (LV) in the predictors matrix that best predict LVs in the response variable. This regression technique reduces data dimensionality, noise, and is computationally fast. Due to the small number of calibration soil samples a full cross-validation technique was applied here. Soil structure, moisture, temperature, and particle size can affect field spectra (Morgan et al., 2009; Shonk et al., 1991). To account for these different physical factors EC and temperature data were incorporated as predictors in the spectral model development. Models were developed using: vis–NIR (350–2200 nm) spectra, EC, temperature and different combinations of the above listed. Due to different ranges and units of the predictors used in the PLS regression, they were modified by autoscaling (mean centered and scaled by 1/SD, where SD is standard deviation) prior to modeling. This transformation assured that all variables have the same weight in estimating the components. For one predictor linear regression was used whereas, for two and three predictors a multiple linear regression was applied as a modeling method.

2.6. Statistical validation

The precision of cross-validated calibration models developed using different spectral regions and combinations of auxiliary data were evaluated using statistical estimates: root mean square error of full-cross validation (RMSECV), being a measure of the error indicating the type of calibration method used; R^2 reflecting explained variance by the model; and the ratio of standard error of prediction to standard deviation (RPD). An RPD classification by Chang and Laird (2002) used for the estimation of model performance classifies RPD values into three groups: RPD > 2 indicating a model with good predictive ability, 1.4 < RPD < 2 for an intermediate model yet to be improved and RPD < 1.4 for a model with no predictive ability.

The best calibration models according to statistical measures were applied to the remaining field spectra to provide point prediction of SOC, clay, silt and sand for the two fields.

2.7. Variogram modeling and map generation

Variogram modeling and interpolation of the predicted soil properties were performed using the ArcGIS version 10.1 software (ESRI, Redlands, CA) including the Geostatistical Analyst extension (ESRI, 2011). Geostatistical analysis of the variograms included nugget, partial sill and range values. Maps of soil properties were generated using ordinary kriging interpolation.

The use of densely spaced data points collected in one direction (following tramlines in the field) can cause a stripping effect when kriging. Therefore, Veris MSP data was averaged in order to create a more grid-like data point distribution. Segments of 6 data points were averaged and the coordinate of the middle point of each segment was used, resulting in a field grid of approximately 12 × 12 m. Data sets with predicted soil properties from the two fields used in kriging interpolation were divided into training and validation data sets comprising 80% and 20% of the total data, respectively, for validating the prediction maps.

3. Results

3.1. General statistics and description of the study sites

The Veris MSP data consisted of measurements acquired at 7307 and 5138 georeferenced data points collected along 34 and 25 transects at fields Voulund1 and Voulund2, respectively. Based on the collected spectral data 15 clusters were defined and one representative calibration soil sample for each cluster was chosen (Fig. 3). This was done for each field separately. General statistics of the wet chemistry soil properties for the calibration samples are shown in Table 1. The two investigated fields are relatively homogenous showing low standard deviations and small ranges of the listed soil properties. Both have a high sand content (mean values of 90%) with a small gradient in SOC (1.4–3.3%) and clay (3–6.7%) and consequently low EC values (0.3–3%). As reported previously by Stenberg et al. (2010) small range and standard deviation of the soil properties may affect the predictive ability of the NIRS models. Thus, the addition of other sensor data (EC and temperature) is expected to improve the calibration models. The improvement is expected especially due to a high correlation between the soil properties of interest and the EC data (Table 2). In Voulund1 the highest reported correlation was between SOC and EC-sh (0.65) and SOC and temperature (0.60). Even higher correlation between SOC and EC was obtained in Voulund2 (0.85). Also high but negative correlation between sand and EC-sh and EC-dp can be seen (0.61 and 0.64, respectively) in Voulund2.

3.2. Calibration results

Calibration models based on EC data only yielded very similar results for SOC content at the two sites, explaining 65% and 69% of the variation with standard errors of 0.43% and 0.34% at Voulund1 and Voulund2, respectively (Table 3 and 4). At both fields temperature data showed no predictive ability for SOC. Vis–NIR spectra used in the PLSR models covered a range between 500 and 2130 nm after noise reduction. Since soil spectra collected by the Ocean Optics sensor (500–1073 nm) were in general of a lower quality than those collected by the Hamamatsu sensor (900–2130 nm), additional PLS models based on the spectral range between 1073 and 2130 nm were also generated and compared to models based on the entire vis–NIR range. Only the best result from the two spectral ranges was reported in Tables 3 and 4. Excluding spectral range between 500 and 1073 nm did not improve SOC calibration models at either of the two sites (data not shown). Nor did the pretreatments thus, absorbance spectra were used. The models based on vis–NIR spectra only provided better results than EC and temperature models at Voulund1 explaining 80% of the variation in SOC with a relatively low RMSECV of 0.26% (Table 3). A lower predictive ability of vis–NIR spectra was reported at Voulund2 site (RMSECV = 0.43 and R^2 = 0.77) (Table 4).

Even though temperature on its own showed no predictive ability for SOC the calibration results in Voulund1 were improved significantly from RMSECV = 0.26, R^2 = 0.80 when using spectra only, to RMSECV = 0.14 and R^2 = 0.94 when combined with the vis–NIR spectra. In Voulund2 the addition of both EC and temperature to vis–NIR spectra resulted in the best SOC model with the lowest RMSECV (0.17%), high correlation (R^2 = 0.93) and RPD of 3.5, indicating an excellent model. Similarly to modeling at Voulund1, the results were improved also significantly after fusing the data as opposed to using single sensor data.

The best calibration models for clay when using data from the individual sensors were obtained using soil spectral data at both sites. Neither EC nor temperature alone could predict clay content. At Voulund1, reducing vis–NIR spectral range to 1073–2130 nm and additional smoothing (Standard Normal Variate correction with de-trending) improved the results for clay prediction producing a RMSECV of 0.34% and the R^2 = 0.76, indicating model with a good predictive ability. At Voulund2, in turn, the reduction of spectral region did not cause model improvement. The vis–NIR model (based on absorbance spectra) resulted in a similar RMSECV (0.39%) to that of Voulund1, but a higher correlation between soil spectra and clay content (R^2 = 0.84).

Further fusion of different sensor data did not increase the predictive ability of clay models at Voulund1. At Voulund2 in turn, the combination of vis–NIR spectral data with temperature improved calibration results significantly in comparison to using spectra only by decreasing the value of RMSECV to 0.20% and increasing the explained variation to 92%.

The highest predictive ability for silt with individual sensor was achieved when using vis–NIR (absorbance) spectra, resulting in RMSECV values of 0.35% and 0.31% and R^2 values 0.82 and 0.86 at Voulund1 and Voulund2, respectively. None of the sensor data combinations could outperform the results of spectral models.

Similarly to silt calibration results sand was best predicted using spectral data only. Low errors of predictions (0.85% and 74%) and high correlations (0.81 and 0.92) were obtained at Voulund1 and Voulund2, respectively. The reduction of used spectral region to 1073–2130 nm gave better results than when using the entire vis–NIR region for sand calibration at Voulund1. Even though, 67% of the variation in sand was predicted using EC data alone at Voulund1, the combination of EC and spectral data did not improve sand model further.

Table 1
General statistics of 15 calibration samples Voulund1 and Voulund2.

	SOC[c]		Clay		Silt		Sand		EC-sh[d]		EC-dp[e]		Temp.[f]	
	V1[a]	V2[b]	V1	V2	V1	V2	V1	V2	V1	V2	V1	V2	V1	V2
Mean	2.32	2.31	4.31	4.48	1.05	1.08	90.67	90.53	1.53	1.56	0.99	1.01	13.46	11.26
Max	3.34	3.27	5.7	6.7	3.3	2.8	93	94	2.96	2.52	2.02	1.67	14.46	13.07
Min	1.37	1.41	3	3.3	0.27	0.14	86	86	0.46	0.88	0.3	0.67	12.42	10.06
Range	1.97	1.86	2.7	3.4	3.03	2.66	7	8	2.5	1.64	1.72	1	2.04	3.01
SD[g]	0.55	0.6	0.72	0.92	0.77	0.79	1.8	2.53	0.6	0.52	0.38	0.3	0.6	0.78

[a] V1, Voulund1.
[b] V2, Voulund2.
[c] SOC, soil organic carbon.
[d] EC-sh, shallow electrical conductivity (0–30 cm).
[e] EC-dp, deep electrical conductivity (0–90 cm).
[f] Temp., soil temperature.
[g] SD, standard deviation.

Table 2
Correlation matrix between soil properties of the 15 calibration samples for Voulund1 and Voulund2 fields.

	Voulund1						
	SOC	Clay	Silt	Sand	EC-sh	EC-dp	Temp.
SOC[a]	1	0.22	0.74	−0.84	0.65	0.49	−0.60
Clay	0.69	1	0.34	−0.56	−0.26	−0.35	0.12
Silt	0.52	0.79	1	−0.87	0.26	0.06	−0.21
Sand	−0.85	−0.93	−0.82	1	−0.34	−0.13	0.42
EC-sh[b]	0.86	0.46	0.28	−0.61	1	0.97	−0.60
EC-dp[c]	0.85	0.46	0.31	−0.64	0.95	1	−0.49
Temp.[d]	0.12	0.05	0.47	−0.29	−0.08	0.04	1
Voulund2							

[a] SOC, soil organic carbon.
[b] EC-sh, shallow electrical conductivity (0–30 cm).
[c] EC-dp, deep electrical conductivity (0–90 cm).
[d] temp., soil temperature.

The combination of different sensor data resulted in calibration improvement for SOC at both sites and clay calibration at Voulund2. Otherwise, it was spectral data which yielded best models.

In all cases, except for clay in Voulund1, additional spectral pretreatment did not improve the final calibration results. This was consistent with the findings by Muñoz and Kravchenko (2011) who reported that the preprocessing methods generally did not improve the calibration results significantly and that they were property and site dependent.

3.3. Variogram modeling and prediction maps

After averaging 735 and 736 data points, respectively, were available for the further mapping. In the last stage of the analysis, randomly selected 80% of the predicted values obtained from the PLS calibration models were used for calculating the experimental variograms for each soil property and each field and to produce kriging maps. Model parameters for the semivariograms of soil properties are shown in Table 5. Spherical models were fitted to all data sets. The variability of the mapped soil properties in Voulund1 was generally lower than for the soil properties in Voulund2 (Table 1) thus, higher ranges were found (Table 5). The nugget variance can be explained by, measurement error, short range variability, and random and inherent variability.

Table 3
Results from the calibration models for Voulund1 field.

Soil property		EC [b]	Temp. [c]	Vis–NIR [d]	EC + temp.	Vis–NIR + EC	Vis–NIR + temp.	Vis–NIR + ec + temp.
SOC [a]	SE[e] /RMSECV [f]	0.43	0.47	0.26	0.35	0.20	0.14	0.16
	R^2	0.65	0.30	0.80	0.62	0.88	0.94	0.93
	NF [g]	–	–	6	–	7	7	7
	RPD [h]	–	–	2.1	–	2.7	3.9	3.4
Clay	SE/RMSECV	0.63	0.69	0.34*	0.66	0.34*	0.43*	0.39*
	R^2	0.09	0.00	0.76*	0.00	0.75*	0.61*	0.68*
	NF	–	–	8*	–	5*	5*	5*
	RPD	–	–	2.1*	–	2.1*	1.6*	1.8
Silt	SE/RMSECV	0.55	0.81	0.35	0.49	0.53	0.45	0.62
	R^2	0.51	0.00	0.82	0.62	0.59	0.70	0.44
	NF	–	–	8	–	9	10	8
	RPD	–	–	2.2	–	1.4	1.6	1.2
Sand	SE/RMSECV	1.06	0.36	0.85*	1.09	1.04	0.86	0.94*
	R^2	0.67	0.18	0.81*	0.66	0.71	0.80	0.76*
	NF	–	–	5*	–	5	5	5*
	RPD	–	–	2.1*	–	1.7	2.1	1.9*

[a] SOC, soil organic carbon.
[b] EC, shallow and deep electrical conductivity.
[c] Temp., soil temperature.
[d] vis–NIR, visible near infrared spectra (500–2130 nm).
[e] SE, standard error of linear regression.
[f] RMSECV, root mean square error of full cross-validation.
[g] NF, number of factors.
[h] RPD, ratio of standard error of prediction to standard deviation.
* Results for spectral models based on the 1073–2130 nm spectral range.

Table 4
Results from the calibration models for Voulund2 field.

Soil property		EC[b]	Temp.[c]	Vis–NIR[d]	EC + temp.	Vis–NIR + EC	Vis–NIR + temp.	Vis–NIR + ec + temp.
SOC[a]	SE[e]/RMSECV[f]	0.34	0.65	0.43	0.69	0.19	0.42	0.17
	R^2	0.69	0	0.77	0.35	0.91	0.57	0.93
	NF[g]	–	–	1	–	9	1	5
	RPD[h]	–	–	1.4	–	3.5	1.6	3.5
Clay	SE/RMSECV	0.98	0.92	0.39	0.96	0.49	0.20	0.32
	R^2	0	0.04	0.84	0	0.74	0.92	0.83
	NF	–	–	5	–	5	9	6
	RPD	–	–	2.3	–	1.9	4.6	2.9
Silt	SE/RMSECV	0.83	0.73	0.31	0.75	0.41	0.45	0.52
	R^2	0	0.15	0.86	0.10	0.74	0.70	0.59
	NF	–	–	9	–	10	10	10
	RPD	–	–	2.5	–	1.9	1.7	1.5
Sand	SE/RMSECV	2.15	2.55	0.74	2.09	0.99	0.84	1.13
	R^2	0.27	0	0.92	0.32	0.86	0.89	0.81
	NF	–	–	6	–	7	8	6
	RPD	–	–	3.4	–	2.5	3	2.2

[a] SOC, soil organic carbon.
[b] EC, shallow and deep electrical conductivity.
[c] Temp., soil temperature.
[d] vis–NIR, visible near infrared spectra (500–2130 nm).
[e] SE, standard error of linear regression.
[f] RMSECV, root mean square error of full cross-validation.
[g] NF, number of factors.
[h] RPD, ratio of standard error of prediction to standard deviation.

Table 5
Parameters for variogram models for soil organic carbon (SOC), clay, silt and sand in Voulund1 and Voulund2 fields.

Soil property	Nugget variance	Partial sill	Nugget/sill	Range (m)	MSEP[a] (%)
Voulund1					
SOC	0.018	0.058	0.24	147.93	0.17
Clay	0.085	0.149	0.36	80.59	0.36
Silt	0.030	0.064	0.32	140	0.20
Sand	0.148	0.213	0.41	182	0.41
Voulund2					
SOC	0.035	0.069	0.34	39.33	0.26
Clay	0.166	0.167	0.49	45.63	0.50
Silt	0.035	0.026	0.57	64.99	0.21
Sand	0.984	0.822	0.54	42	1.21

[a] MSEP, mean standard error of prediction in kriging validation.

Cambardella et al. (1994) used three nugget-to-sill classes to define distinct classes of spatial dependence for the soil variables: with a ratio ⩽25% the variable was considered strongly spatially dependent, with the ratio between 25% and 75% the variable was considered moderately spatially dependent and with the ratio >75% it was considered weakly spatially dependent. Following this classification, the nugget-to-sill ratios in our study showed a moderate spatial dependence for all soil properties except for SOC in Voulund1 where strong spatial dependence was found. This may be a result of soil-forming processes and other factors such as long-term soil fertilization and cultivation practices. Generally lower nugget-to-sill ratios were reported for soil properties at Voulund1 indicating a higher spatial dependency.

Even if the investigated sites were relatively homogenous, the kriging maps based on 80% of the sensor data were able to detect small scale variability and spatial patterns of all the predicted soil properties within the two fields (Fig. 4). In Voulund1, the distribution of SOC was strongly and negatively correlated with sand, and moderately and positively correlated with silt (except for the south-eastern part of the field). This is consistent with Table 2 showing the measured correlation coefficients for these soil properties. In Voulund2, mapped soil properties have a more similar spatial trend and show much higher correlations. Also here, the spatial patterns of SOC variability are strongly and negatively correlated with sand content, whereas a positive correlation between clay and silt is clearly visible. Validation of kriging interpolation was performed using the remaining 20% of the data. Lower mean standard error of predictions were obtained for the soil properties interpolated in Voulund1 than in Voulund2 (Table 5) most probably due to generally lower variability of the soil properties present in this data set (Table 1). Good validation results of kriging were obtained for soil properties with low mean errors of predictions except for the interpolation of silt content (Table 5).

4. Discussion

The enhanced improvement of SOC and clay calibrations based on fused sensor data can be explained by the high correlations between the two soil properties and the sensor data. Yet, despite a good correlation between sand and EC the addition of EC did not improve the predictive abilities of sand calibration models based on spectral data. Nevertheless, the fact that the calibration models for SOC and clay based on spectral data were inferior to those based on fused data may be due to moisture effects on soil spectra. Organic matter and clay minerals have distinct finger prints relating to several functional groups including the hydroxyl group. The effects of moisture content on soil spectral can be observed across the visible and NIR regions of the electromagnetic spectrum (Knadel et al., 2014). In the visible range soil becomes darker with increasing soil moisture content. This is also where OM absorption bands can be found. Moreover, water has strong absorption bands in the NIR region with the dominant absorption near 1400 and 1900 nm (Ben-Dor, 2002). Key components in organic matter have a peak near 1930 nm. The strong water absorption band near 1900 nm can mask this peak associated with organic functional groups. The spectral features of clay minerals are due to overtones and combination of the molecular vibration modes of OH functional groups in crystal lattice or absorbed water (Ben-Dor, 2002). The major mineral diagnostic regions are located

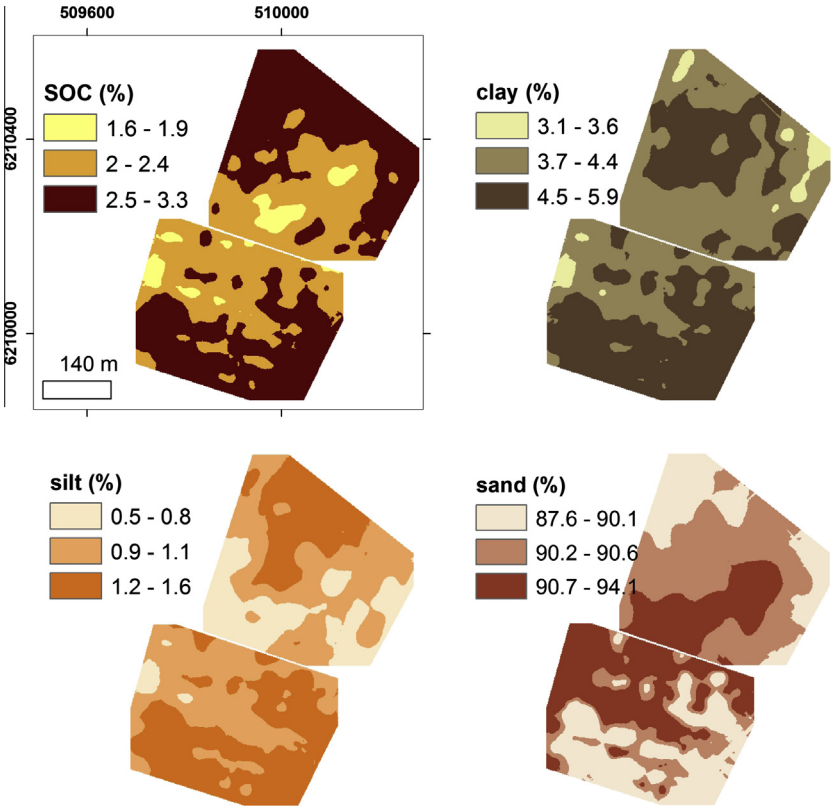

Fig. 4. Prediction maps of soil organic carbon and texture for the two fields (2 column fitting image).

between 1300-1400 nm, 1800-1900 nm and 2200-2500 nm and hold information on clay minerals such as smectite, kaolin or illite (Clark, 1999). Due to the fact that absorption bands related to clay minerals can be found at the same wavelengths as those of water, excessive moisture content in the soil can mask the signals from clay minerals. Additionally, the spectrophotometer used in the MSP has a spectral range only extending to 2200 nm, not including the upper part of the NIR range where some of the absorption bands related to clay minerals are located. This can explain why both clay and SOC calibration results were improved when soil spectra were fused with supplementary data.

A comparison of our calibration results with other studies is not straightforward. Even though the use of mobile sensor platforms for soil properties mapping is increasingly reported in the literature the included sensor data and the soil properties in focus are not readily comparable. Some studies combined on-the-go measurements with laboratory or remotely sensed data for a range of soil properties. Yet, we found no studies using mobile sensing of soils or even on field moist soils targeted for silt and sand prediction. To ease the comparison we focused mainly on the mobile platform studies including NIR sensors, possibly supported by other types of sensors (Table 6).

Only the study reported by Knadel et al. (2011) used the Veris sensor platform supporting the same sensors (vis–NIR, EC and temperature). The best predictive ability was reported in their study for a fusion of spectral and EC data. However, much higher RMSECV (5.89%) was obtained in their study and was attributed to the bimodal distribution and the extremely wide range of SOC (Table 6). The application of Veris platform including solely vis–NIR or NIR sensors for soil properties mapping was reported in several studies. Debaene et al. (2013) tested the potential of on-the-go estimation of SOC of mineral soils in Poland using Veris vis–NIR sensor. They compared the result from the mobile system to the maps based on soil samples scanned in the laboratory obtaining similar results from the two approaches. The PLS models, however, for SOC resulted in lower error of prediction (0.19%) and a lower correlation (R^2 = 0.70) probably due generally lower SOC content. In another study two NIR sensors (Veris shank-based and airbone hyperspectral vis–NIR sensors) were used and compared for carbon mapping (McCarty et al., 2010). Low predictive ability of the validation results were obtained for the shank-based sensor (R^2 = 0.53). Christy (2008) used the Veris NIR sensor (920–1718 nm) to determine several soil attributes. He obtained acceptable prediction of soil OM for eight fields in Kansas with a RDP value of 1.7 (Table 6). Total carbon was analyzed on a subset of 20 samples to determine the correlation with OM thus the comparison is not possible. The lower predictive ability of the mobile system in comparison to ours might be explained by a lower spectral range. Shen et al. (2013) used also a Veris mobile NIR sensor to predict both SOC and clay in a field in Michigan, USA. Similar to the results from our study better predictions were obtained for SOC than for clay (Table 6). Despite the higher range of SOC in the study by Shen et al., 2013, calibration results were comparable to our results when using spectral data in model development (R^2 values were not given). However, the performance of their clay calibration model was significantly lower (RPD = 1.1). The better predictive ability for clay models in our study may be explained by a much lower variation in this property, the higher range of spectrophotometer, and might also be due to different moisture conditions at the two of our study sites. Much worse results, however, were obtained by Bricklemeyer and Brown (2010) who applied the Veris vis–NIR sensor for SOC and clay content mapping in eight wheat fields in Montana. The Montana results were consistent with those by Christy (2008) but the mobile spectrophotometer was not able to capture SOC variability. Not even semi-quantitative levels of validation for SOC could be achieved (Table 6). The

Table 6
Comparison of mobile sensor fusion results for selected soil properties mapping.

	N[d]	Study area	Predictors	Sensor vendor	Min	Max	SD[e]	Calibration method	RMSEP[f]	R^2	RPD[g]	Reference
SOC[a]	15	1 field (13.7 ha)	Vis–NIR (350–2200 nm) Temp.	Veris Tech.	1.4	3.3	0.55	PLS[h], full cross-validation	0.14	0.94	3.9	Present study
Clay			NIR (1073–2200 nm)		3	5.7	0.72		0.34	0.76	2.1	
SOC	15	1 field (12.7 ha)	Vis–NIR (350–2200 nm) EC, Temp.		1.4	3.3	0.6		0.17	0.93	3.5	
Clay			Vis–NIR (350–2200 nm) Temp.		3.3	6.7	0.92		0.20	0.92	4.6	
SOC	15	1 field (12 ha)	Vis–NIR (350–2200 nm) EC, temp.		1.2	38.3	13.9		5.89	0.84	2.3	Knadel et al. (2011)
SOC	20	1 field (22 ha)	Vis–NIR (350–2200 nm)		0.65	2	–		0.19	0.70	–	Debaene et al. (2013)
SOC	50	1 field (7000m^2)	Vis–NIR (306–1711)	Zeiss Corona 45, Geramny	0.7	6	0.95		0.48	0.74	1.97	Mouazen et al. (2007)
OM[b]	119	8 fields	NIR (920–1718 nm)	Veris Tech.	0.51	4.54	0.88	PLS, one-field-out	0.52	0.67	1.7	Christy (2008)
SOC	50	2 fields			0.7	1.33	–	PLS-O[i]	0.14	0.66	–	Muñoz and Kravchenko (2011)
	50	(12 ha each)			0.7	1.48	–	PLS-O	0.15	0.44	–	
SOC	765	8 fields,	Vis–NIR		0.6	2.72	0.32	PLS, one-field-out	0.35	0	0.9	Bricklemeyer and Brown (2010)
Clay	311	(16 ha each)	(350–2220 nm)		5.5	48.3	9.14		9.03	0.17	1	
SOC	64	1 field	NIR		0.55	2.9	0.4	PLS, cross-validation	0.2	–	2	Shen et al. (2013)
Clay		(50 ha)	(920–1718 nm)		2	21	4.2		3.9	–	1.1	
TC[c]	72 per field	2 fields (total 8.94 ha)	Vis–NIR (310–1700 nm)	Zeiss Corona 45, Geramny	0.79	3.13	0.46	PLS, full cross-validation	0.15	0.89	3.1	Kodaira and Shibusawa (2011)
SOC	85	1 field (50 ha)	Vis–NIR (350–220 nm)	Veris Tech.	0.55	2.89	–	MLR[j]	0.19	0.70	–	Huang et al. (2007)
			Vis–NIR (350–220 nm), moisture, silt, clay, slope and WI		0.55	2.89	–	MLR	0.13	0.88	–	
SOC	304	5 fields	NIR (920–2225 nm)		0.5	2.6	–	PLS	0.18	0.53	–	McCarty et al. (2010)

[a] SOC, soil organic carbon mapping.
[b] OM, organic matter.
[c] TC, total carbon.
[d] *N*, number of calibration samples.
[e] SD, standard deviation.
[f] RMSEP, root mean square of prediction.
[g] RPD, ratio of standard error of prediction to standard deviation.
[h] PLS, partial least square regression.
[i] PLS-O, partial least squares regression leaving-one-outlier out.
[j] MLR, multiple regression.

authors explained the poor results with the low range and variation in SOC, with their range being equivalent to almost half of the variation in SOC in our study. The results from the clay models were improved, however, in comparison to those of SOC (RPD = 1) but still presented no predictive ability. According to the authors this small improvement was caused by a higher variability in clay (SD = 9.1).

Results from other NIR platforms than Veris were also reported. In the study by Mouazen et al. (2007) a mobile vis–NIR sensor with a soil penetration unit was developed and used for different soil attributes (total C, pH and P). Lower predictive ability for the online vis–NIRS determination of organic C content was obtained (RMSEP = 0.48, R^2 = 0.74) than in the current study. Their measurements were based on spectral data only (Table 6). Nevertheless, when comparing their results with our SOC calibration based on spectral data only, higher predictive ability of the PLS models in the current study was achieved (RPD > 2). This might be due to the fact that the mobile system of Mouazen et al. (2007) employed a spectrophotometer covering more limited spectrum (306–1711 nm) and thus missing other important regions for SOC determination. Moreover, the variability of SOC within their study field was higher (SD = 0.95), causing a higher error of prediction. Kodaira and Shibusawa (2011) used another specially developed mobile sensor platform consisting of a vis–NIR sensor and tested the performance of this system on 2 fields in Japan. Their results for total carbon were better than those for SOC presented in our study which might be due to a very high sampling density (ca. 18 samples per ha) whereas only 1 sample per ha was used here.

Fewer studies were reported on the actual fusion of the on-the-go obtained spectral information with other sensor data. Huang et al. (2007) reported on the fusion of Veris-based NIRS measurements and Landsat imagery with topography for SOC prediction (Table 6). When using only NIR spectra they found a lower, yet acceptable predictive ability than presented in our study, consistent with the findings by other authors investigating the potential of NIRS in the SOC range between 0.5% and 2.9%. Huang et al. (2007) improved their results by adding complementary information such as moisture content, texture and topography indices. The sensor of Christy (2008) was used for soil carbon mapping together with topography and aerial photographs in a more recent study by Muñoz and Kravchenko (2011). Unsatisfactory results were obtained for two adjacent fields in Michigan. Mobile

vis–NIR measurements performed worse than topographical and aerial vis–NIR data. Poor predictive ability of the models was explained by low carbon values and the limited range, being the lowest of all the compared studies (Table 6). Unfortunately no information on the SOC variation was provided. Moreover, high sand content and differences in moisture content among the two fields were suspected to degrade the models.

In summary, differences in calibration performance of the MSPs can be attributed to two main factors: the type of fused instrumentation and the actual differences in soil variability among the studied fields. Higher spectral range of the NIR sensors and the additional fusion with auxiliary data result in higher predictive ability of the models. Too low contents and limited ranges of the selected soil properties in the data sets can lead to degraded results of the calibration models, but at the same time too high variability may result in high prediction errors.

5. Conclusions

The mobile sensor platform provided an efficient tool for predicting and mapping SOC and soil texture for two fairly homogenous, sandy, agricultural fields in Denmark. With the use of the MSP we were able to obtain densely spaced measurements in the fields. Robust calibration models based on sensor data were generated for all soil properties providing significant labor savings compared to traditional soil texture mapping.

The effect of sensor data fusion was dependent on the soil properties studied and their correlation with sensor data. Improved calibration results due to sensor fusion were obtained for SOC and clay with a decrease in the mean errors of prediction of almost 50% in comparison to using single sensor. This might be due to the fact that the absorption features of the two soil properties are mostly affected by variable moisture content. Thus, by integrating the spectral data with other sensor measurements this NIRS methodological issue may be partly overcome.

Moreover, high resolution field maps generated on the basis of sensor measurements were able to depict the small spatial variability of the soil properties present within the two fields. The results of this study show a considerable potential of data fusion in field-scale soil characterization for applications such as precision agriculture. However, it is important to underline that the general predictive ability of mobile sensors depends on soil spatial variability, the concentrations, and the ranges of the soil properties. Additionally, factors related to the uncontrolled field conditions can affect the quality of in-situ data resulting in a poor performance or even a failure of the mobile sensors application. Thus, more work on overcoming the factors affecting on-the-go acquired data is still needed.

Acknowledgements

Financial support for this work came from the HOBE – research center for hydrology (http://www.hobecenter.dk/) via a grant from the Villum Foundation and from the SINKS project.

References

Ben-Dor, E., 2002. Quantitative remote sensing of soil properties. Adv. Agron. 75 (75), 173–243.
Bricklemeyer, R.S., Brown, D.J., 2010. On-the-go VisNIR: potential and limitations for mapping soil clay and organic carbon. Comput. Electron. Agri. 70, 209–216.
Broge, N.H., Thomsen, A.G., Greve, M.H., 2004. Prediction of topsoil organic matter and clay content from measurements of spectral reflectance and electrical conductivity. Acta Agri. Scandinavica Sec. B – Soil Plant Sci. 54, 232–240.
Cambardella, C.A., Moorman, T.B., Nova, J.M., Parkin, T.B., Karlen, D.L., Turco, R.F., Konopka, A.E., 1994. Field-scale variability of soil properties in central Iowa soils. Soil Sci. Soc. Am. J. 58, 1501–1511.
Chang, C.W., Laird, D.A., 2002. Near-infrared reflectance spectroscopic analysis of soil C and N. Soil Sci. 167, 110–116.
Christy, C.D., 2008. Real-time measurement of soil attributes using on-the-go near infrared reflectance spectroscopy. Comput. Electron. Agri. 61, 10–19.
Clark, R.N., 1999. Spectroscopy of rocks and minerals and principles of spectroscopy. In: Rencz, A.N. (Ed.), Remote Sensing for the Earth Sciences. Manual of Remote Sensing. John Wiley & Sons, UK, Chichester, pp. 3–58.
Corwin, D.L., Lesch, S.M., 2003. Application of soil electrical conductivity to precision agriculture: theory, principles, and guidelines. Agron. J. 95, 455–471.
Corwin, D.L., Lesch, S.M., 2005. Apparent soil electrical conductivity measurements in agriculture. Comput. Electron. Agri. 46, 11–43.
Dane, J.H., Topp, G.C., 2002. Methods of Soil Analysis: Part 4 Physical Methods. Soil Science Society of America Inc., Madison, Wisconsin, USA, pp. 278–283.
Debaene, G., Niedzwiecki, J., Pecio, A., 2013. On-the-go mapping of soil organic carbon content in Western Poland. In: Proceedings of the 3rd Global Workshop on Proximal Soil Sensing, Potsdam-Bornim, 2013, pp. 248–251.
Domsch, H., Giebel, A., 2004. Estimation of soil textural features from soil electrical conductivity recorded using the EM38. Precision Agric. 5, 389–409.
ESRI, 2011. ArcGIS Desktop: Release 10. 1. Environmental Systems Research Institute, Redlands, CA.
Huang, X.W., Senthilkurnar, S., Kravchenko, A., Thelen, K., Qi, J.G., 2007. Total carbon mapping in glacial till soils using near-infrared spectroscopy, Landsat imagery and topographical information. Geoderma 141, 34–42.
Hummel, J.W., Gaultney, L.D., Sudduth, K.A., 1996. Soil property sensing for site-specific crop management. Comput. Electron. Agri. 14, 121–136.
Knadel, M., Thomsen, A., Greve, M.H., 2011. Multisensor on-the-go mapping of soil organic carbon content. SSSAJ 75, 1799.
Knadel, M., Peng, Y., Schelde, K., Thomsen, A., Deng, F., Greve, M.H. 2013. Optimal sampling and sample preparation for NIR-based prediction of field scale soil properties, poster at EGU General Assembly 2013, Vienna, 7–11 April 2013.
Knadel, M., Deng, F., Alinejadian, A., De Jonge, L.W., Moldrup, P., Greve, M.H., 2014. The effects of moisture conditions – from wet to hyper dry – on visible near-infrared spectra of Danish reference soils. SSSAJ 78, 422–433.
Kochanowski, R.G., Gregorich, E.G., Van Wesenbeeck, I.J., 1988. Estimating spatial variations of soil water content using noncontacting electromagnetic inductive methods. Canad. J. Soil Sci. 68, 715–722.
Kodaira, M., Shibusawa, S., 2011. Dozen parameters soil mapping using the real-time soil sensor. In: Proceeding of the second global workshop on proximal soil sensing. Proceedings of the 2nd global workshop on proximal soil sensing, McGill University Press, Montreal, Canada, 2011, pp. 88–91.
Lück, E., Gebbers, R., Ruehlmann, J., Spangenberg, U., 2009. Electrical conductivity mapping for precision farming. Near Surface Geophys. 7, 15–25.
Lund, E.D., Christy, C.D., Drummond, P., 1999. Practical applications of soil electrical conductivity mapping. In: Proceedings of the Second European Conference on Precision Agriculture, Odense, Denmark, 1999, pp. 771–779.
Madsen, H.B., Nørr, A.H., Holst, K.Aa., 1992. The Danish Soil Classification. Atlas of Denmark I, Reitzel, Copenhagen.
Malley, D.F., Martin, P.D., Ben-Dor, E., 2004. Application in analysis of soils. In: Roberts, C.A. et al. (Eds.), Near-Infrared Spectroscopy in Agriculture. American Society of Agronomy, Crop Science Society of America, Soil Science Society of America Publishers, pp. 729–784.
McCarty, G., Hively, W.D., Reeves, J., Lang, M., Lund, E., Weatherbee, O., 2010. Infrared sensors to map soil carbon in agricultural ecosytems. In: Viscarra Rossel, R.A. et al. (Eds.), Proximal Soil Sensing. Springer, pp. 165–176.
Moral, F.J., Terron, J.M., da Silva, J.R.M., 2010. Delineation of management zones using mobile measurements of soil apparent electrical conductivity and multivariate geostatistical techniques. Soil & Tillage Res. 106, 335–343.
Morgan, C.L.S., Waiser, T.H., Brown, D.J., Hallmark, C.T., 2009. Simulated in situ characterization of soil organic and inorganic carbon with visible near-infrared diffuse reflectance spectroscopy. Geoderma 151, 249–256.
Mouazen, A.M., Maleki, M.R., De Baerdemaeker, J., Ramon, H., 2007. On-line measurement of some selected soil properties using a VIS-NIR sensor. Soil & Tillage Res. 93, 13–27.
Muñoz, J.D., Kravchenko, A., 2011. Soil carbon mapping using on-the-go near infrared spectroscopy, topography and aerial photographs. Geoderma 166, 102–110.
Rinnan, R., Rinnan, A., 2007. Application of near infrared reflectance (NIR) and fluorescence spectroscopy to analysis of microbiological and chemical properties of arctic soil. Soil Biol. Biochem. 39, 1664–1673.
Schelde, K., Ringgaard, R., Herbst, M., Thomsen, A., Friborg, T., Soegaard, H., 2011. Comparing evapotranspiration on rates estimated from atmospheric flux and TDR soil moisture measurements. Vadose Zone J. 10, 78–83.
Schirrmann, M., Gebbers, R., Kramer, E., Seidel, J., 2011. Evaluation of soil sensor fusion for mapping macronutrients and soil pH. In: Proceedings of the 2nd Global Workshop on Proximal Soil Sensing, Montreal, Canada, 2011, pp. 48–51.
Shen, Z.-Q., Shan, Y.-J., Peng, L., Jiang, Y.-G., 2013. Mapping of total carbon and clay contents in glacial till soil using on-the-go near-infrared reflectance spectroscopy and partial least squares regression. Pedosphere 23, 305–311.
Shonk, G.A., Gaultney, L.D., Schulze, D.G., Van Scoyoc, G.E., 1991. Spectroscopic sensing of soil organic matter content. Trans. ASAE 34, 1978–1984.
Stenberg, B., Viscarra Rossel, R.A., 2010. Diffuse reflectance spectroscopy for high-resolution soil sensing. In: Rossel, R.A.V. et al. (Eds.), Proximal Soil Sensing. Springer, pp. 29–47.
Stenberg, B., Viscarra Rossel, R.A., Mouazen, A.M., Wetterlind, J., 2010. Visible and near infrared spectroscopy in soil science. Adv. Agron. 107, 163–512.

Sudduth, K.A., Kitchen, N.R., Wiebold, W.J., Batchelor, W.D., Bollero, G.A., Bullock, D.G., Clay, D.E., Palm, H.L., Pierce, F.J., Schuler, R.T., Thelen, K.D., 2005. Relating apparent electrical conductivity to soil properties across the north-central USA. Comput. Electron. Agri. 46, 263–283.

Viscarra Rossel, R.A., Adamchuk, V.I., Sudduth, K.A., McKenzie, N.J., Lobsey, C., 2011. Proximal soil sensing: an effective approach for soil measurements in space and time. In: Sparks, D.L. (Ed.), Advances in Agronomy. Academic Press, Burlington, pp. 237–282.